



HAL
open science

Impact of aerosol direct radiative forcing on the radiative budget, surface heat fluxes, and atmospheric dynamics during the heat wave of summer 2003 over western Europe : a modeling study

Jean-Christophe Pere, Marc Mallet, Véronique Pont, Bertrand Bessagnet

► To cite this version:

Jean-Christophe Pere, Marc Mallet, Véronique Pont, Bertrand Bessagnet. Impact of aerosol direct radiative forcing on the radiative budget, surface heat fluxes, and atmospheric dynamics during the heat wave of summer 2003 over western Europe : a modeling study. *Journal of Geophysical Research: Atmospheres*, 2011, 116, pp.D23119. 10.1029/2011JD016240 . ineris-00963328

HAL Id: ineris-00963328

<https://ineris.hal.science/ineris-00963328>

Submitted on 16 Jun 2022

HAL is a multi-disciplinary open access archive for the deposit and dissemination of scientific research documents, whether they are published or not. The documents may come from teaching and research institutions in France or abroad, or from public or private research centers.

L'archive ouverte pluridisciplinaire **HAL**, est destinée au dépôt et à la diffusion de documents scientifiques de niveau recherche, publiés ou non, émanant des établissements d'enseignement et de recherche français ou étrangers, des laboratoires publics ou privés.

Copyright

Impact of aerosol direct radiative forcing on the radiative budget, surface heat fluxes, and atmospheric dynamics during the heat wave of summer 2003 over western Europe: A modeling study

J. C. Péré,¹ M. Mallet,² V. Pont,² and B. Bessagnet¹

Received 12 May 2011; revised 8 September 2011; accepted 14 October 2011; published 15 December 2011.

[1] In this work, an off-line coupling between the chemistry-transport model CHIMERE (associated with an aerosol optical module) and the meteorological model Weather Research and Forecasting (WRF) is used to study (1) the direct radiative forcing of pollution aerosols during the heat wave of summer 2003 over western Europe and (2) the possible feedbacks of this direct radiative forcing on the surface-atmosphere system. Simulations performed for the period 7–15 August 2003 reveal a significant decrease of daily mean solar radiation reaching the surface ($\Delta F_{\text{BOA}} = -(10\text{--}30) \text{ W/m}^2$) because of back scattering at the top of the atmosphere ($\Delta F_{\text{TOA}} = -(1\text{--}12) \text{ W/m}^2$) and also absorption of solar radiation by polluted particles ($\Delta F_{\text{atm}} = + (5\text{--}23) \text{ W/m}^2$). During daytime, the aerosol surface dimming induces a mean reduction of both sensible (16 W/m^2) and latent (21 W/m^2) heat fluxes emitted by the terrestrial surface, resulting in a radiative cooling of the air near the surface (up to 2.9 K/d at noon). Simultaneously, the absorption of solar energy by aerosols causes an atmospheric radiative heating within the planetary boundary layer reaching 1.20 K/d at noon. As a consequence, the direct radiative effect of aerosols is shown to reduce both the planetary boundary layer height (up to 30%) and the horizontal wind speed (up to 6%); that may have contributed to favor the particulate pollution during the heat wave of summer 2003.

Citation: Péré, J. C., M. Mallet, V. Pont, and B. Bessagnet (2011), Impact of aerosol direct radiative forcing on the radiative budget, surface heat fluxes, and atmospheric dynamics during the heat wave of summer 2003 over western Europe: A modeling study, *J. Geophys. Res.*, 116, D23119, doi:10.1029/2011JD016240.

1. Introduction

[2] The interaction of aerosols with solar radiation, through both scattering and absorption mechanisms, tends to modify the global radiative energy balance of the Earth. This is the so-called aerosol direct radiative forcing (ADRF) [Yu *et al.*, 2006]. By scattering solar radiation, aerosols can decrease the amount of solar energy reaching the ground, thus resulting in a cooling of the Earth's surface [Trenberth *et al.*, 2009]. In addition, aerosols can absorb solar energy causing a warming of the atmospheric layer where aerosols are located [Wang *et al.*, 2009]. At the regional scale, the direct radiative forcing due to aerosols can exceed, in terms of intensity, the radiative forcing due to greenhouse gases and can lead to complex climate feedback mechanisms [Ramanathan, 2001; Forster *et al.*, 2007; Shindell and Faluvegi, 2009].

[3] In recent years, interest in studying the radiative effects of aerosols and their impacts on the regional climate has grown considerably [Ramanathan and Carmichael, 2008;

Kulmala *et al.*, 2011]. Several measurements campaigns were conducted in different regions of the world affected by important concentrations of atmospheric particles from different origins (urban/industrial, smoke and mineral dust): south Africa (SAFARI 2000 [Keil and Haywood, 2003]), India (INDOEX [Ramanathan, 2001]), Asia (Ace-Asia [Huebert *et al.*, 2003] and East-AIRE [Li *et al.*, 2007]), West Africa (AMMA [Redelsperger *et al.*, 2006]), Mexico (MILAGRO [Molina *et al.*, 2010]). In parallel with field campaigns, numerical models were used to assess the climate impact of aerosols showing that the ADRF can contribute, with the aerosol semidirect and indirect effects, to important feedbacks on the water cycle and atmospheric dynamics [Tummon *et al.*, 2010; Zhang *et al.*, 2010]. For example, the radiative cooling of the ocean surface related to the presence of the Indian pollution plume [Meywerk and Ramanathan, 2002] may decrease by 5% (in annual mean) the water evaporation at the ocean surface, resulting in a possible diminution of rainfalls over the northern part of the Indian Ocean [Ramanathan, 2001]. Also, the weakening of the convective activity in the lower troposphere due to the radiative effect of dust particles may cause a reduction of precipitations in the Sahelian region [Konaré *et al.*, 2008; Solmon *et al.*, 2008; Mallet *et al.*, 2009]. Furthermore, the ADRF has been shown to be one of the factors that could affect air temperature and wind intensity [Gong *et al.*, 2007; Zhang *et al.*, 2010] or modify the

¹Institut National de l'Environnement Industriel et des Risques, Verneuil en Halatte, France.

²Laboratoire d'Aérodologie, Université de Toulouse, CNRS, Toulouse, France.

photosynthetically active radiation causing some changes in crop fields [Matsui *et al.*, 2008; Mercado *et al.*, 2009]. In spite of these recent efforts, our comprehension of aerosol impact on the regional climate is still uncertain, as highlighted by Forster *et al.* [2007]. In particular, one potential source of uncertainty in the estimation of the ADRF and its climate feedbacks concerns the model representation of the aerosol optical properties and their influence on the radiative budget in the atmosphere [Boucher *et al.*, 1998; Solmon *et al.*, 2008; Loeb, 2010]. For instance, Randles and Ramaswamy [2010] suggested that the hydrological cycle over southern Africa is very sensitive to the total amount of aerosol solar absorption. Aerosol optical properties depend especially on their size and chemical composition as well as their microphysical and chemical evolution during their transport through the atmosphere. For example, some studies showed that solar absorption by aerosols can increase when black carbon particles become coated by a shell of secondary species during their transport from emissions sources [Bond *et al.*, 2006; Zhang *et al.*, 2008; Lack *et al.*, 2009; Shiraiwa *et al.*, 2009].

[4] Up to now, many studies have focused on characterizing aerosol optical properties and direct radiative forcing over Europe [Lyamani *et al.*, 2006; Roger *et al.*, 2006; Hodzic *et al.*, 2007; Marmer *et al.*, 2007; Norris and Wild, 2007; Elias and Roujean, 2008; Saha *et al.*, 2008; Santos *et al.*, 2008; Di Biagio *et al.*, 2009; Calvo *et al.*, 2010] but few of them have studied the possible feedback of the ADRF on the European regional climate [Hohenegger and Vidale, 2005; Zanis, 2009].

[5] The present study aims at investigating the shortwave ADRF of pollution particles and its potential feedbacks on the European regional climate during the heat wave of summer 2003. This episode, characterized by important concentrations of primary (black and organic carbon) and secondary (sulphates, nitrates, secondary organics) aerosols [Vautard *et al.*, 2007a] and by large concentrations of ozone [Guerova and Jones, 2007] over western Europe, represents an interesting opportunity to understand how the ADRF can modify the atmospheric dynamics over European polluted regions.

[6] For such an evaluation, a methodology based on an off-line coupling between the chemistry transport model CHIMERE [Vautard *et al.*, 2001; Bessagnet *et al.*, 2004] and the meteorological model WRF [Skamarock *et al.*, 2001] have been developed. In this approach, aerosol optical properties (aerosol optical thickness, single scattering albedo and asymmetry parameter) are first computed by the chemistry transport model for a core-shell aerosol mixing state, following the methodology developed by Péré *et al.* [2009, 2010]. The assumption of a core-shell mixing of particles is related to the previous work of Péré *et al.* [2009] dealing with the mixing state of aerosols during the European heat wave of summer 2003 in which they clearly showed that the core-shell mixing approach had better ability to reproduce the absorption properties of particles during this specific period. Second, aerosol optical properties are used as inputs in radiative transfer scheme of the meteorological model WRF to evaluate the ADRF and its impact on the European regional climate. An advantage of such methodology is an accurate estimation of the aerosol direct radiative effects by using two sophisticated models with reasonable computation time. Section 2 describes the configuration of each model as well as the development of

their off-line coupling. In section 3 are discussed the impacts of particles on the radiative budget, near-surface air temperature, surface heat fluxes, heating/cooling rates profiles, wind intensity and planetary boundary layer height. Finally, conclusions and outlooks of this work are given in section 4.

2. Model Description and Off-Line Coupling

2.1. Description of the CHIMERE Model

2.1.1. Aerosol Module

[7] The air quality model CHIMERE is a state-of-the-art 3-D chemistry transport model calculating the concentrations of gas phase and aerosol species [Vautard *et al.*, 2001]. The dynamics and gas phase parts of the model [Schmidt *et al.*, 2001] have successively been improved [Vautard *et al.*, 2003, 2005a]. The full model documentation can be found at <http://www.lmd.polytechnique.fr/chimere/>. In this study, the CHIMERE grid ranges from 37°N to 54°N in latitude and from -9°E to 22°E in longitude with 36 km resolution.

[8] The aerosol module, described by Bessagnet *et al.* [2004], calculates concentrations of 10 chemical species: sulphates, nitrates, ammonium, primary organic and black carbon (OC and BC), secondary organic aerosols (SOA), sea salt, natural and anthropogenic dust and water. The particle size distribution ranges from about 40 nm to 10 μm and is distributed into 12 bins. Dynamical processes influencing aerosol population such as nucleation of sulphuric acid, coagulation, condensation/evaporation, adsorption/desorption, wet and dry deposition and scavenging are taken into account.

[9] Anthropogenic gaseous and particulate emissions (CO, SO₂, NH₃, CH₄, NMVOC, primary particulate matter) are taken from EMEP inventory and soil dust are locally produced within the domain after Vautard *et al.* [2005a]. OC and BC emissions are issued from the methodology of Junker and Liousse [2008] study. Particulate matter and trace gases (such as CO, VOC, NO, NO₂, etc.) released by important wildfires that affected western Europe during summer 2003 are taken into account according to the methodology described by Hodzic *et al.* [2007]. Production of sea salt is calculated using wind intensity at the ocean surface following the formulation of Monahan [1986]. SOA formation is represented according to oxidation of relevant precursors and gas particle partitioning of the condensable oxidation products. The chemical scheme includes precursors of biogenic (such as isoprene, terpene, etc.) and anthropogenic (such as benzene, toluene, etc.) origin. The gas particle partitioning formulation of Pun *et al.* [2006] has been adapted to the SOA formation mechanism implemented in CHIMERE [Bessagnet *et al.*, 2009]. VOC and NO emissions from vegetation are calculated using the Model of Emissions of Gases and Aerosols from Nature (MEGAN) [Guenther *et al.*, 2006]. Boundary conditions are issued from monthly climatologies, calculated over the 2000–2004 period, of global chemistry transport models MOZART [Horowitz *et al.*, 2003] for gaseous pollutants and LMDzT-INCA [Dentener *et al.*, 2006; Textor *et al.*, 2006] for aerosols. Meteorological data (3-D wind, air temperature, humidity, etc.) are provided by the Weather Research and Forecasting model (WRF) at 36 km resolution over Europe.

[10] The CHIMERE model has been extensively evaluated in simulating gaseous and particulate pollutants at the European [Bessagnet *et al.*, 2004; Honoré *et al.*, 2008] and urban [Hodzic *et al.*, 2005; Monteiro *et al.*, 2007] scales. It has also

Table 1. Wavelength-Dependent Complex Refractive Indexes of Each Aerosol Species Used in the CHIMERE Optical Module^a

Species	Complex Refractive Index (n-ik)		
	300–400 nm	600 nm	999 nm
Nitrate	1.53-i0.006 ^b	1.53-i0.006	1.53-i0.006
Ammonium	1.52-i0.0005 ^c	1.52-i0.0005	1.51-i0.0005
Sulfate	1.44-i10 ^{(-8)c}	1.43-i2.6 × 10 ⁻⁸	1.50-i × 10 ⁻⁸
OC	1.45-i0.001 ^c	1.45-i0.001	1.45-i0.001
BC	1.87-i0.569 ^d	1.87-i0.569	1.87-i0.569
SOA	1.45-i0.001 ^c	1.45-i0.001	1.45-i0.001
Sea salt	1.45-i0.0056 ^c	1.45-i5 × 10 ⁻⁵	1.45-i1.2 × 10 ⁻⁴
Dust	1.52-i0.008 ^c	1.51-i0.008	1.50-i0.008
Water	1.34-i2 × 10 ^{(-9)c}	1.33-i3.4 × 10 ⁻⁸	1.32-i1.43 × 10 ⁻⁶

^aHere n and k are the real and imaginary parts of the complex refractive index, respectively. OC, organic carbon; BC, black carbon.

^bSee *d'Almeida et al.* [1991].

^cSee *Krekov* [1993].

^dSee *Marley et al.* [2001].

been used in several studies including the analysis of the European air quality during the 2003 heat wave episode [*Vautard et al.*, 2005b] and participated in model intercomparison exercises [*Vautard et al.*, 2007b].

2.1.2. Modeling Aerosol Optical Properties

[11] The aerosol optical properties are calculated from CHIMERE outputs of aerosol chemical composition and size distribution following the methodology described and evaluated by *Péré et al.* [2009, 2010]. The aerosol optical thickness (AOT), single scattering albedo (SSA), and asymmetry parameter (g) required in radiative transfer calculations are evaluated using Mie theory for a core-shell aerosol mixing.

[12] In the core-shell mixing, each particle is assumed to be composed by a core of primary organics, black carbon and mineral dust surrounded by a shell of secondary species (sulphate, nitrate, ammonium, secondary organics), sea salt and water. In each size bin, the complex refractive index of the core ($\overline{m}_{\text{core}}$) and the shell ($\overline{m}_{\text{shell}}$) have been determined using a volume average procedure [*Lesins et al.*, 2002]:

$$\overline{m}_{\text{core}} = \sum_{i=1}^{i=N_{\text{core}}} f_{i,\text{core}} \times m_{i,\text{core}} \quad (1)$$

$$\overline{m}_{\text{shell}} = \sum_{i=1}^{i=N_{\text{shell}}} f_{i,\text{shell}} \times m_{i,\text{shell}} \quad (2)$$

where $f_{i,\text{core/shell}}$ and $m_{i,\text{core/shell}}$ are the volume fraction and the complex refractive index of species i in the core/shell, respectively. N_{core} and N_{shell} are the total number of species in the core (BC, OC, and dust) and the shell (sulphate, nitrate, ammonium, SOA, sea salt, and water), respectively.

[13] In our simulations, the volume of the core and the shell can vary with the size of the particle as the volume of chemical species can differ from the size of one bin to another because of physical processes influencing aerosol population such as nucleation, coagulation, condensation/evaporation, adsorption/desorption and deposition.

[14] The complex refractive index of the core and the shell are then used within the Mie algorithm for n-layered sphere of *Wu and Wang* [1991] to calculate the absorption and scattering coefficients of a core-shell particle. The wavelength-dependent refractive indexes of each chemical species used to perform optical calculations are reported in Table 1.

2.2. Description of the WRF Model

[15] The Weather Research and Forecasting (WRF) model is a state-of-the-art numerical weather prediction and atmospheric simulation system designed for both research and operational applications. The version 3.1 released in April 2009 is used in this study for a domain covering the western Europe with an horizontal resolution of 36 km (the same as CHIMERE) and for 20 vertical levels ranging from 40 m to about 20 km above ground level. The full WRF model documentation can be downloaded at <http://www.mmm.ucar.edu/wrf/users/downloads.html>. Boundaries and initial meteorological conditions come from global analysis performed with the Global Forecast System (GFS) [*Kalnay et al.*, 1998]. The characteristics of the land surface such as soil type, vegetation index, albedo or surface topography are provided by the National Center for Atmospheric Research (NCAR) and available at <http://dss.ucar.edu/datasets/ds083.2/>. Sea surface temperatures are updated every 6 h from the National Centers for Environmental Prediction (NCEP) reanalysis [*Kalnay et al.*, 1996].

[16] The WRF model has many parametrizations for the main physical schemes implemented: microphysics of clouds, planetary boundary layer (PBL), surface-atmosphere interactions and radiation. The major physics options used in this study include the WRF single-moment five-class scheme of *Hong et al.* [2006] for the microphysics module, the Kain-Fritsch cumulus parametrization [*Kain*, 2004], the NOAA land surface module of *Chen and Dudhia* [2001] and the Yonsei University PBL scheme [*Hong et al.*, 2006; *Hong*, 2007] in which the PBL top is defined using a critical bulk Richardson number of zero.

[17] The radiative transfer module uses as input monthly means surface albedo from NCEP. The radiation scheme provides longwave and shortwave upward/downward radiative fluxes at the ground (bottom of the atmosphere (BOA)) and at the top of the atmosphere (TOA). Thus, we infer the atmospheric heating and cooling due to radiative flux convergence and divergence. Within the atmosphere, radiation respond to clouds and water vapor distribution, carbon dioxide, ozone and trace gases as well as the presence of aerosols through an off-line coupling with the CHIMERE model. For shortwave radiation, the Goddard model [*Chou and Suarez*, 1994], including 11 spectral bands from 0.2 to 6 μm is used, while for longwave radiation, the Rapid Radiative Transfer model (RRTM) [*Mlawer et al.*, 1997] including 16 spectral bands from 6 to 1000 μm has been chosen. Aerosol impacts on longwave radiation, such as sea salt and mineral dust, are not taken into account in RRTM.

[18] The WRF model associated with the Goddard radiative transfer code has been widely used to study the shortwave radiative forcing of aerosols at a regional scale [*Fast et al.*, 2006; *Chapman et al.*, 2009; *Mashayekhi et al.*, 2009; *Zhang et al.*, 2010; *Zhao et al.*, 2010].

2.3. Off-Line Coupling Between CHIMERE and WRF

[19] The methodology developed in this study consists of an off-line and one-way coupling between CHIMERE and WRF. Meteorological input parameters required by CHIMERE such as 3-D wind, air temperature or relative humidity are provided by WRF. Secondly, aerosol optical properties (AOT, SSA, and g) are simulated using CHIMERE for an aerosol core-shell

Table 2. Climatology of Aerosol Optical Properties for Free Troposphere and Stratosphere Issued From *Hess et al.* [1998]^a

	Free Troposphere (6–12 km)				Stratosphere (12–20 km)			
	0.3 μm	0.4 μm	0.6 μm	0.99 μm	0.3 μm	0.4 μm	0.6 μm	0.99 μm
AOT	0.025	0.019	0.011	0.006	0.010	0.007	0.005	0.001
SSA	0.94	0.94	0.94	0.94	1	1	1	1
g	0.7	0.7	0.7	0.7	0.7	0.7	0.7	0.7

^aAOT, aerosol optical thickness; SSA, single scattering albedo.

mixing [*Péré et al.*, 2009, 2010]. Finally, meteorological simulations are performed using aerosol optical properties (AOT, SSA, and g) as inputs in the WRF radiative transfer module to take into account the impact of particles on solar radiation and its potential feedback on meteorology. In the simulations, the time steps of the CHIMERE and WRF models as well as the time step of their coupling are 1 h. It should be noted that this methodology enables only the investigation of climate feedbacks due to the ADRF. To account for the aerosol indirect effects, a complete online and two-way coupling between WRF and CHIMERE would be required.

[20] Here we focus our study on the impact of fine polluted aerosols on shortwave solar radiation. Aerosol optical properties are calculated at 0.3, 0.4, 0.6 and 0.99 μm and then interpolated on the shortwave radiation bands (0.2–6 μm) of the WRF radiative transfer module. AOT, SSA and g are estimated for the eight vertical layers of the CHIMERE model ranging from 40 m to about 6 km above ground level. For higher altitude, a climatology of optical properties for free troposphere and stratosphere [*Hess et al.*, 1998] has been used (Table 2).

[21] To estimate the ADRF and its feedback on meteorology, two parallel simulations have been performed for the heat wave period of 7–15 August 2003: one including the ADRF and the other without. The calculations of radiative fluxes integrated over the shortwave range are performed at 1 h interval. From these fluxes, we compute the ADRF at the bottom of the atmosphere (ΔF_{BOA}) and at the top of the atmosphere (ΔF_{TOA}) as follows:

$$\Delta F_{\text{BOA}} = F_{\text{BOA}}^w - F_{\text{BOA}}^o$$

$$\Delta F_{\text{TOA}} = -(F_{\text{TOA}}^w - F_{\text{TOA}}^o)$$

where F_{BOA}^w and F_{BOA}^o are the net radiative flux at the surface simulated with (w) and without (o) aerosols, respectively. F_{TOA}^w and F_{TOA}^o are the net radiative flux simulated at the top of the atmosphere with (w) and without (o) aerosols, respectively. Finally, we compute the atmospheric radiative forcing (ΔF_{atm}) by using the following relation [*Roger et al.*, 2006]:

$$\Delta F_{\text{atm}} = \Delta F_{\text{TOA}} - \Delta F_{\text{BOA}} \quad (3)$$

where ΔF_{atm} represents the absorption of solar radiation by aerosols within the atmospheric layer.

3. Results and Discussion

3.1. Aerosol Direct Radiative Forcing Over Western Europe

[22] Because of the low variability of aerosol emissions sources, associated with stagnant meteorological conditions

during the period studied [*Vautard et al.*, 2007a], results presented hereafter will be time-averaged between 7 and 15 August 2003.

[23] The exceptional nature of this specific episode in terms of aerosol optical thickness can be estimated by comparing (Figure 1) the mean observed AOT (at 440 nm) averaged over 7–15 August for the year 2003 (in red) and for the period 2004–2010 (in blue) at different AERONET stations spread over western Europe (no data available at IMC Oristano for the period 2004–2010). Except over Hamburg and Leipzig, the mean AERONET AOT (at 440 nm) observed between 7 and 15 August 2003 at the other stations (0.42–0.64) is a factor of 2–2.5 larger than AOT obtained for the same period averaged over the years 2004–2010 (0.18–0.30). This result was previously highlighted by *Hodzic et al.* [2006], who showed an increase by a factor of 2 of the AOT observed by the Polder sensor over Europe during the first part of August 2003 as compared to other summer months.

[24] Simulations of AOT (400 nm), SSA (400 nm), and g (400 nm) with corresponding photometric observations at some AERONET stations are displayed in Figure 2. According to *Dubovik et al.* [2000, 2002] and *Holben et al.* [2001], uncertainties on AERONET retrievals (for $\lambda \geq 440$ nm) are equal to ± 0.01 for the AOT, $\pm 5\%$ for the asymmetry parameter and ± 0.03 if AOT (440 nm) > 0.2 and ± 0.07 otherwise for the single scattering albedo. The predicted AOT is shown to be underestimated by a factor of 2–3 over northern France, Benelux, and Germany, which could be due to uncertainties in estimating the aerosol size distribution and total particles load, as previously highlighted by *Péré et al.* [2010]. In contrast, the model correctly simulates the aerosol optical thickness over the southern part of the domain and particularly in southeastern

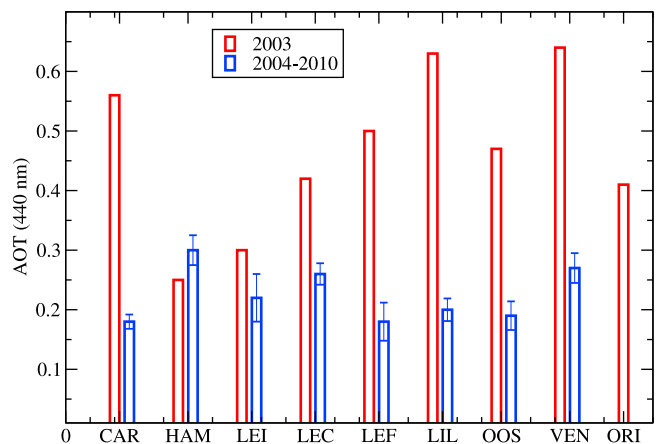


Figure 1. Mean observed aerosol optical thickness (AOT) (440 nm) averaged over 7–15 August for the year 2003 (in red) and for the period 2004–2010 (in blue) at different Aerosol Robotic Network (AERONET) stations spread over western Europe (no data are available at IMC Oristano for the period 2004–2010). The interannual variability (standard deviation) is indicated by error bars. OOS, Oostende (2.93°E, 51.23°N); LEF, Le Fauga (1.29°E, 43.38°N); HAM, Hamburg (9.58°E, 53.34°N); ORI, IMC Oristano (8.30°E, 39.54°N); LEC, Lecce University (18.06°E, 40.20°N); VEN, Venice (12.30°E, 45.18°N); CAR, Carpentras (5.03°E, 44.04°N); LIL, Lille (3.08°E, 50.36°N); LEI, IFT Leipzig (12.26°E, 51.20°N).

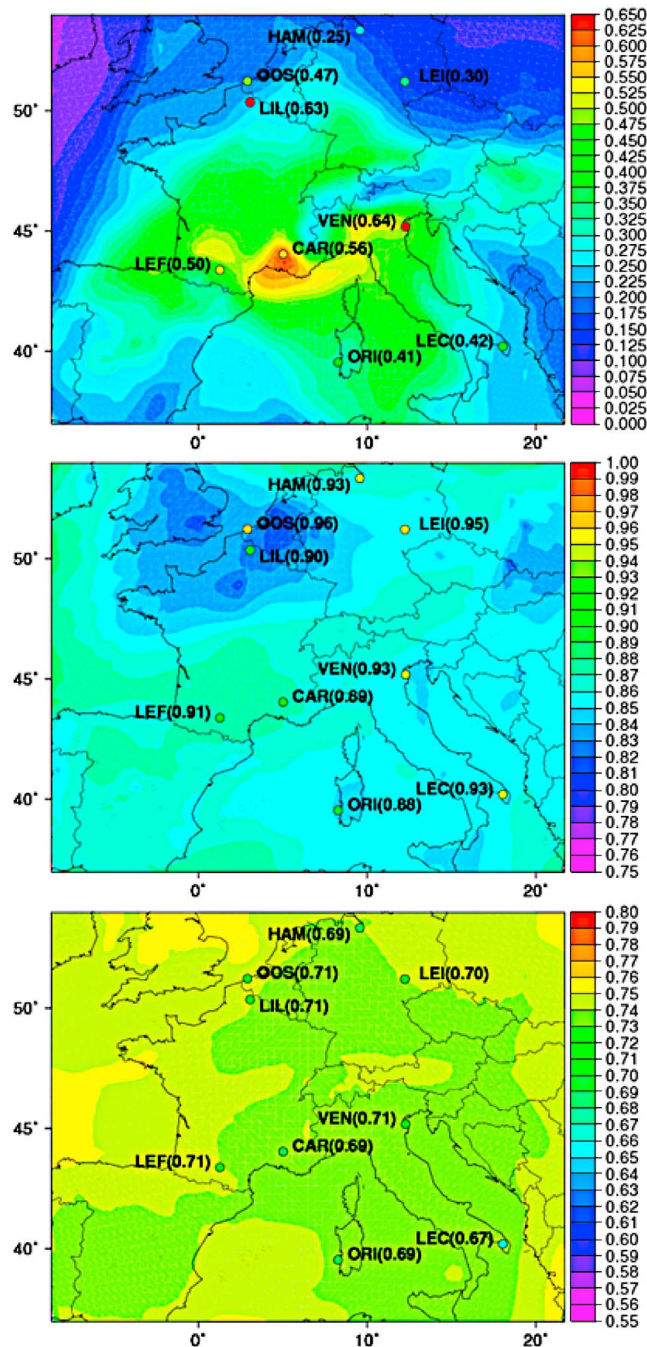


Figure 2. (top) AOT, (middle) single scattering albedo (SSA), and (bottom) g averaged between 7 and 15 August 2003 from CHIMERE simulations at 400 nm and retrieved by AERONET at 440 nm (colored circles).

France with modeled values ($AOT_{\text{chimere}}(400 \text{ nm}) = 0.55\text{--}0.65$) in good agreement with AERONET observations at Carpentras ($AOT_{\text{aeronet}}(440 \text{ nm}) = 0.56 \pm 0.01$).

[25] Results of simulated SSA show values ranging from 0.80 to 0.87 (at 400 nm) over a large part of the domain. Over southeastern France, the estimated SSA (0.86–0.87 at 400 nm) is in rather good agreement with mean AERONET values at Carpentras (0.89 ± 0.03 at 440 nm). A much more detailed evaluation of the SSA modeled by CHIMERE during

the heat wave of summer 2003 over western Europe is reported by *Péré et al.* [2009]. In this study, a statistical comparison of modeled and observed SSA over 10 AERONET sites clearly shows that, for most of the sites studied, results for the core-shell mixing are in better agreement with AERONET values with smaller biases, as compared to other mixing approaches.

[26] Comparisons of simulated asymmetry parameter to AERONET observations indicate that biases are rather small over the domain (less than 10%) (Figure 2). Second, simulated AOT, SSA, and g are used to evaluate the impact of particles on shortwave radiative fluxes. Results for the ADRF (integrated between 0.2 and 6 μm) simulated at the ground (ΔF_{BOA}), at the top of the atmosphere (ΔF_{TOA}) and within the atmospheric layer (ΔF_{atm}) and averaged between 7 and 15 August 2003 are displayed on Figure 3. Simulated ADRF are clearly important over regions characterized by large AOT: Milan area, the Mediterranean basin and southern France ($AOT_{\text{chimere}}(400 \text{ nm}) = 0.55\text{--}0.65$). In term of intensity, we can see that the modeled ADRF is much larger at the surface than at TOA. Over southeastern France and the Mediterranean Basin, aerosols induce a mean decrease of net solar energy reaching the surface of 30 W/m^2 ($\approx 50 \text{ W}/\text{m}^2/AOT(400 \text{ nm})$) and an increase of net backscattered radiation at the top of the atmosphere of (10–12) W/m^2 ($\approx (17\text{--}20) \text{ W}/\text{m}^2/AOT(400 \text{ nm})$). We can clearly see here the impact of internal mixing of black carbon, which induces an important absorption capacity of the particle leading to a strong atmospheric forcing over southeastern France and the Mediterranean Basin ($\Delta F_{\text{atm}} = 23 \text{ W}/\text{m}^2 \approx 38 \text{ W}/\text{m}^2/AOT(400 \text{ nm})$).

[27] From measurements of microphysical and optical aerosol properties obtained during the ESCOMPTE campaign, *Mallet et al.* [2006] and *Roger et al.* [2006] simulated values of ADRF over the Marseille/Fos-Berre area ($\Delta F_{\text{BOA}} = -(24\text{--}47) \text{ W}/\text{m}^2 \approx -(50\text{--}65) \text{ W}/\text{m}^2/AOT(440 \text{ nm})$, $\Delta F_{\text{TOA}} = -(6\text{--}12) \text{ W}/\text{m}^2 \approx -(12\text{--}18) \text{ W}/\text{m}^2/AOT(440 \text{ nm})$) close to the ones modeled in our study. *Zanis* [2009] obtained, in a modeling exercise, instantaneous surface ADRF (at noon) between $-10 \text{ W}/\text{m}^2$ and $-70 \text{ W}/\text{m}^2$ ($\approx -(30\text{--}80) \text{ W}/\text{m}^2/AOT(500 \text{ nm})$) during the heat wave episode that affected eastern Europe in summer 2000.

[28] Similarly, our results are comparable with values obtained during recent campaigns such as “the Atmospheric Brown Cloud Gosan campaign” over Korea ($\Delta F_{\text{BOA}} = -21 \text{ W}/\text{m}^2 \approx -83 \text{ W}/\text{m}^2/AOT(500 \text{ nm})$, $\Delta F_{\text{TOA}} = -8 \text{ W}/\text{m}^2 \approx -33 \text{ W}/\text{m}^2/AOT(500 \text{ nm})$) [Takamura et al., 2007] and MILAGRO (Megacity Initiative-Local and Global Research Observations) over Mexico ($\Delta F_{\text{BOA}} = -22 \text{ W}/\text{m}^2 \approx -30 \text{ W}/\text{m}^2/AOT(400 \text{ nm})$, $\Delta F_{\text{TOA}} = -5 \text{ W}/\text{m}^2 \approx -10 \text{ W}/\text{m}^2/AOT(400 \text{ nm})$) [Schmidt et al., 2010]), which were dedicated to the study of polluted aerosols.

[29] As illustrated in Figure 4, the ADRF affects the near-surface air temperature with a mean decrease (averaged between 7 and 15 August 2003) ranging from 0.1 to 0.3 K in southern France, northeastern Spain and the PÔ valley. This decrease reaches 0.35 K over southeastern France, where the modeled ADRF is important.

[30] During the heat wave episode of summer 2000 over eastern Europe, *Zanis* [2009] highlighted, by using a simplified aerosol module, a nonnegligible aerosol feedback on cloud cover and atmospheric circulation leading to a significant impact on near-surface air temperature ($-1.2 \text{ K} <$

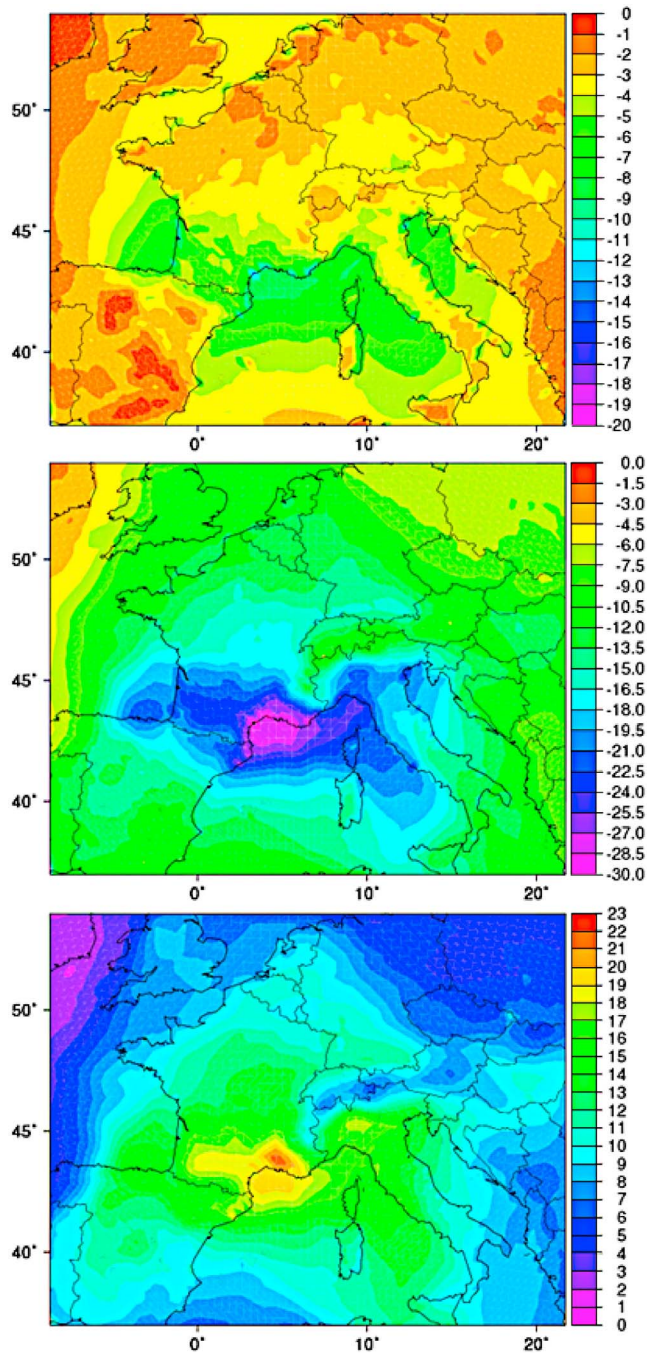


Figure 3. Aerosol direct radiative forcing (in W/m^2), averaged between 7 and 15 August 2003, simulated (top) at the top of the atmosphere (ΔF_{TOA}), (middle) at the ground (ΔF_{BOA}), and (bottom) within the atmospheric layer (ΔF_{atm}).

$\Delta T_{2m} < +1.2$ K, at noon). In parallel, our results are comparable with those obtained over United States by *Zhang et al.* [2010] during summertime ($\Delta T = -0.37$ K) over areas where the presence of particles leads to a decrease of net solar radiation at the surface by 15% (in monthly mean for July 2001). It is noteworthy in Figure 4 that aerosol impact on the 2 m temperature is not always correlated with the respective pattern of the surface ADRF (Figure 3)

indicating the complexity and the nonlinearity of mechanisms involved. For example, the decrease of near-surface air temperature over some parts of northeastern Spain ($\Delta T \simeq 0.20\text{--}0.29$ K) associated with a moderate surface direct radiative forcing ($\Delta F_{\text{BOA}} \simeq -(13\text{--}18) \text{ W/m}^2$) is similar to the decrease of temperature modeled over southeastern France ($\Delta T \simeq 0.25\text{--}0.35$ K) for a surface radiative forcing much stronger ($\Delta F_{\text{BOA}} \simeq -(25\text{--}30) \text{ W/m}^2$). Near-surface air temperature mainly depends on incident solar flux, sensible and latent heat fluxes emitted by the terrestrial surface, aerosol solar absorption near the ground and atmospheric circulation. Hence, the resulting effect of these different mechanisms on the 2 m temperature can vary from a region to another, as previously shown by *Zanis* [2009] over eastern Europe.

[31] In turn, this reduction of air temperature near the ground associated with a potential heating of the atmospheric layer ($\Delta F_{\text{atm}} > 0$, Figure 3) may disturb the atmospheric dynamics such as the development of the planetary boundary layer and may affect the latent and sensible heat fluxes emitted by the terrestrial surface. To further investigate these points, we have focused our simulations over southeastern France, where the ADRF and its impact on near-surface air temperature are pronounced during the period studied.

3.2. Aerosol Direct Radiative Forcing and Its Feedback on Atmospheric Dynamics Over Southeastern France

[32] The studied area is located between $4.1^\circ\text{E}\text{--}6.1^\circ\text{E}$ and $43.00^\circ\text{N}\text{--}44.30^\circ\text{N}$ and includes the cities of Marseille, Avignon, and Carpentras (Figure 5). First, we can see in Figure 6 that the spectral dependence of the modeled AOT (in the visible–near-infrared region), averaged between 7 and 15 August 2003, for the site of Avignon is marked by a decrease from 0.60 to 0.20 (at 400 and 999 nm, respectively). This result is in good agreement with corresponding AERONET observations, indicating that CHIMERE is able to rather well reproduce the particles load as well as the aerosol size distribution over this specific region.

[33] Second, Figure 7 displays the vertical profiles of the modeled aerosol extinction and absorption coefficients (in m^{-1}) averaged between 12 and 13 h for the studied period. We can see that aerosol extinction and absorption are maximum near the ground where particles are emitted and then decrease rapidly up to 500 m. Above, they decrease gradually until an altitude of 8 km from which they become negligible.

[34] Before studying the ADRF and its feedback on the regional atmospheric dynamics, we have compared simulated shortwave (SW) radiative fluxes at the surface with pyranometers measurements issued from the Baseline Surface Radiation Network (BSRN). Figure 8 presents, for each day of the studied period, the total SW flux at the surface (averaged between 5 and 18 h) modeled by WRF (without and with aerosols) and observed at the BSRN station of Avignon. First, we can see a large overestimation of the observed SW solar flux at the surface during the 8, 14, and 15 August 2003 for the simulations including or not the impact of aerosols on solar extinction ($32\% < \text{biases} < 90\%$). For these days affected by cloudy conditions, some uncertainties in modeling cloud processes and their interactions with solar radiation could be one of the reasons for such a discrepancy. For the other days of interest, the estimated biases between the cal-

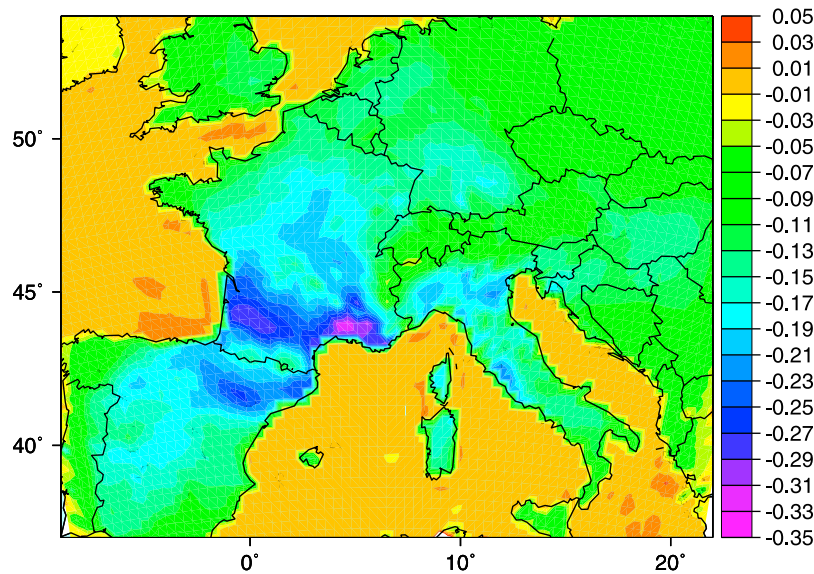


Figure 4. Impact of the aerosol direct radiative forcing on the 2 m temperature (in kelvin), averaged between 7 and 15 August 2003.

culated and measured SW fluxes are shown to be small when taking into account the aerosol solar extinction ($-0.1\% < \text{biases} < 8\%$).

[35] In a second time, we have investigated the ADRF and its impact on the regional atmospheric dynamics. Results presented hereafter are (1) time averaged between 7 and 15 August 2003 and (2) spatially averaged over the studied area.

[36] In Figure 9 are reported the ADRF (integrated between 0.2 and 6 μm) at the ground, TOA and within the atmospheric layer and its feedback on near-surface air temperature and sensible and latent heat fluxes emitted by the surface. As previously shown, aerosols reduce significantly the solar energy reaching the surface ($\Delta F_{\text{BOA}} = -26 \pm 5 \text{ W/m}^2$) by reflection to space ($\Delta F_{\text{TOA}} = -7 \pm 2 \text{ W/m}^2$) and

by absorption of solar radiation ($\Delta F_{\text{atm}} = +19 \pm 5 \text{ W/m}^2$). This ADRF decreases near-surface air temperature by $0.30 \pm 0.06 \text{ K}$ over this specific region.

[37] The reduction of solar radiation reaching the ground due to the presence of particles also affects the surface energy balance, as illustrated in Figure 9. In response to the decrease of total surface solar radiation at the ground, the sensible and latent heat fluxes emitted by the terrestrial surface are reduced in presence of particles, compared to the simulation without the ADRF. We can note that the decrease of the latent heat flux is less pronounced than the decrease of the sensible heat flux, suggesting that the aerosol impact on the moisture gradient is less significant than its impact on the temperature gradient, at the timescale of the simulation. This finding was previously underlined by *Fan et al.* [2008] in their modeling

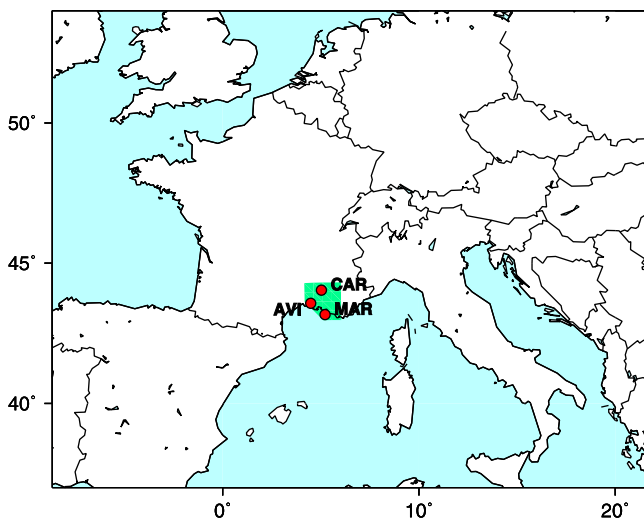


Figure 5. Location of the studied area (in green) including the cities of Marseille (MAR), Avignon (AVI), and Carpentras (CAR).

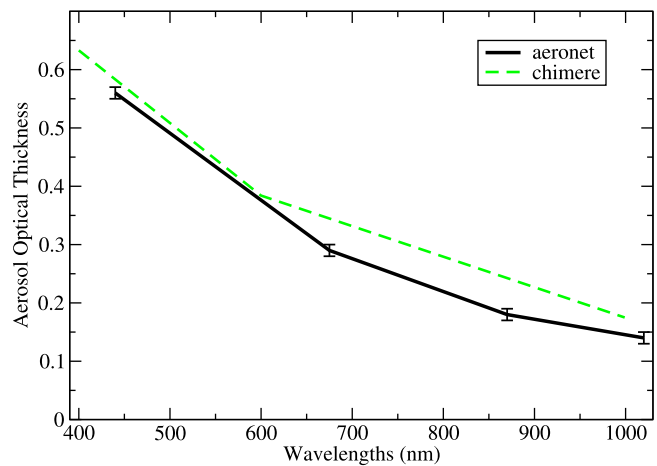


Figure 6. Wavelength dependence of the AOT (averaged between 7 and 15 August 2003) modeled by CHIMERE with corresponding AERONET observations at the site of Avignon. The error bars represent the uncertainty range of AERONET AOT (± 0.01 [see *Dubovik and King, 2000*]).

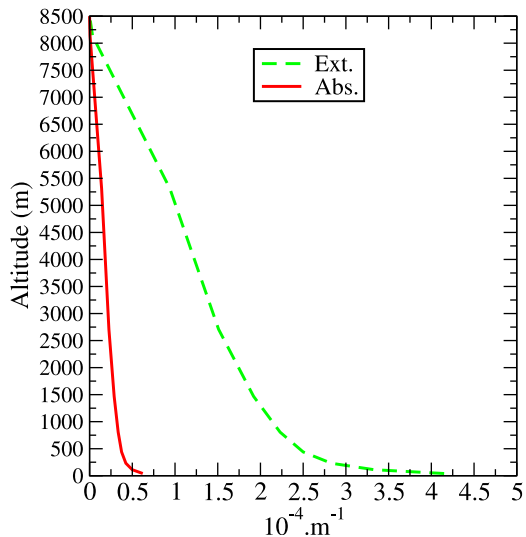


Figure 7. Vertical profiles of the modeled aerosol extinction (Ext.) and absorption (Abs.) coefficients (in m^{-1}) averaged between 12 and 13 h for the studied period.

study of the aerosol direct and semidirect radiative effect over Houston (US).

[38] Our simulations report a mean reduction in the sensible and latent heat flux of $16 \pm 2 \text{ W/m}^2$ (10%) and $21 \pm 2 \text{ W/m}^2$ (18%), respectively. These values are comparable with the ones simulated by *Pandithurai et al.* [2008] for the sensible heat flux (-22 W/m^2) obtained from photometric measurements over India ($\text{AOT}(500 \text{ nm}) = 0.50$, $\text{SSA}(500 \text{ nm}) = 0.90$), in case of a mixture of mineral dust with fine anthropogenic aerosols. For biomass burning aerosols, *Wang and Christopher* [2006] reported a decrease of 6.2 W/m^2 (in daily mean) for both the sensible and latent heat fluxes related to a smaller AOT (0.18 at 550 nm). During an

intense dust outbreak over western Africa ($\text{AOT}(550 \text{ nm}) = 0.8\text{--}1.2$), *Mallet et al.* [2009] reported a significant instantaneous reduction in the sensible heat flux reaching $100\text{--}150 \text{ W/m}^2$ (at noon).

[39] This decrease in sensible and latent heat fluxes emitted by the surface due to the presence of particles leads to a loss of radiative heating in the atmospheric layer. In parallel, the absorption of solar shortwave radiation by aerosols leads to a gain of radiative heating where particles are located. These two effects can be estimated by the terrestrial cooling and solar heating rate (in K/d) averaged between 12 and 13 h (Figure 10), respectively. Aerosols induce a radiative heating of the lower troposphere between 0.65 and 1.20 K/d with a maximum of radiative heating at the bottom of the boundary layer, in agreement with the modeled vertical profiles of aerosol absorption displayed in Figure 7. Above an altitude of 6 km, the solar heating rate gradually decreases to become negligible at 8 km.

[40] For comparisons, *Rajeev et al.* [2010] modeled a mean daytime solar heating rate of 0.8 K/d ($\text{AOT}(500 \text{ nm}) = 0.52$, $\text{SSA}(500 \text{ nm}) = 0.90$) during particulate pollution episodes affecting southern India. In parallel, *Saha et al.* [2008] obtained an important solar heating rate over southeastern France (2 K/d in average) because of the dominance of absorbing aerosols during their study ($\text{SSA}(525 \text{ nm}) = 0.7\text{--}0.8$). Finally, a smaller heating rate has been found during the Indian premonsoon season by *Kedia et al.* [2010] (0.4 K/d in average between March and May 2006), despite a moderate aerosol loading ($\text{AOT}(500 \text{ nm}) = 0.32$), as the chemical composition of particles was dominated by scattering species.

[41] In parallel, we can see in Figure 10 that the reduction of the latent and sensible heat fluxes emitted by the surface due to the presence of particles also induces an important radiative cooling of the lower part of the boundary layer reaching, between 12 and 13 h, 2.9 K/d. This result is comparable with the terrestrial cooling rate simulated by

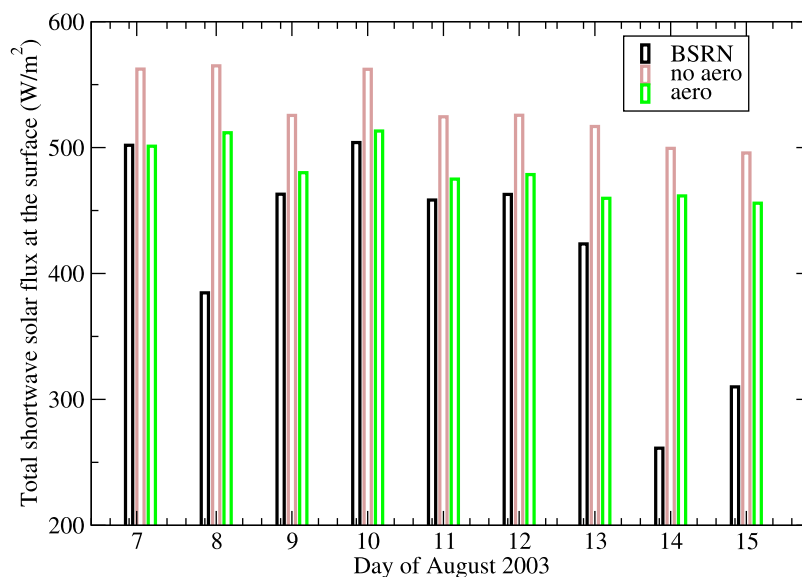


Figure 8. Total shortwave solar flux at the surface (averaged between 5 and 18 h) modeled by Weather Research and Forecasting (WRF) without and with aerosols and observed at the Baseline Surface Radiation Network (BSRN) station of Avignon for each day of the studied period.

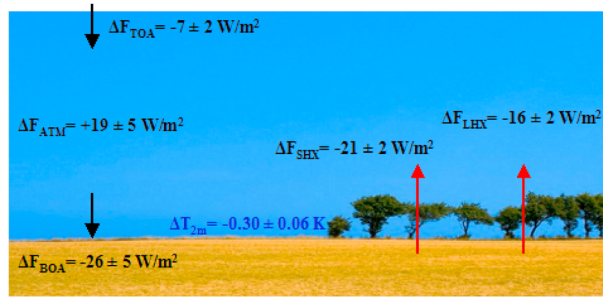


Figure 9. Aerosol direct radiative forcing at the top of the atmosphere (ΔF_{TOA}), at the surface (ΔF_{BOA}), and within the atmospheric layer (ΔF_{ATM}) and its feedbacks on near surface air temperature (ΔT_{2m}) and sensible (ΔF_{SHX}) and latent (ΔF_{LHX}) heat fluxes emitted by the surface. Results are displayed as follows: mean (over the domain and studied period) \pm standard deviation.

Wendisch *et al.* [2008] from measurements of aerosol extinction (lidar, photometer) and absorption (absorption spectrophotometer) over southeastern China.

[42] It is clearly shown in Figure 10 that values of the terrestrial cooling rate are dominant in the lower part of the boundary layer while the solar heating ones due to absorbing particles are dominant above an altitude of 200 m. The consequences could be a possible stabilizing effect in the planetary boundary layer (PBL) that may reduce convective mixing and PBL height.

[43] The potential dispersion of polluted air masses over an area is related to two variables: (1) The first is the PBL height; the more the PBL is developed the more the pollutants are vertically diluted. (2) The second is the horizontal wind speed integrated over the PBL height as a measurement of the horizontal transport of pollutants. The product of these two variables is the so-called ventilation index of the atmosphere [Holzworth, 1972].

[44] Figure 11 shows that the radiative effect of particles causes a reduction of the PBL height during daytime ranging from 40 to 203 m (8%–30%) with the largest decrease simulated at midday (between 12 and 14 h) when the PBL is well developed (Figure 11).

[45] Such a result has also been obtained by Wendisch *et al.* [2008] who reported a reduction of 10%–20% (during daytime) of the PBL height by using a combination of measurements (aerosol optical properties, PBL height estimation from lidar) and modeling studies (PBL dynamic model associated with a radiative transfer code) over southeastern China.

[46] Moreover, the radiative effect of aerosols also induces a decrease of the horizontal wind speed (integrated over the PBL height) during the afternoon (≈ 11 –17 h), with a maximum of reduction reaching 6% between 14 and 15 h (Figure 11). This reduction in horizontal wind speed due to the ADRF could be the consequence of a weakening of the turbulent mixing associated with a shallower boundary layer, as previously highlighted by Park *et al.* [2010] who showed a 20% reduction in horizontal wind speed associated to a decrease of surface solar flux of 200 W/m^2 in presence of an Asian dust layer.

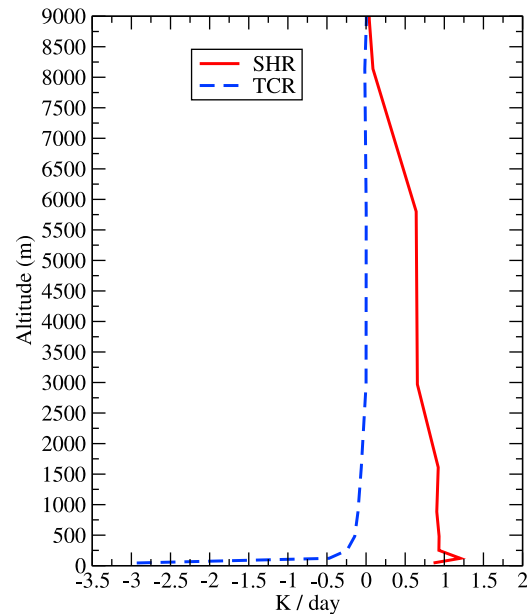


Figure 10. Modeled solar heating (SHR) and terrestrial cooling (TCR) rate (in K/d), averaged between 12 and 13 h.

[47] Finally, the ventilation index of the air (on average over daytime) is found to be reduced by 14% because of the reduction of both the PBL height and the horizontal wind speed, compared to an atmosphere without aerosols. Such a

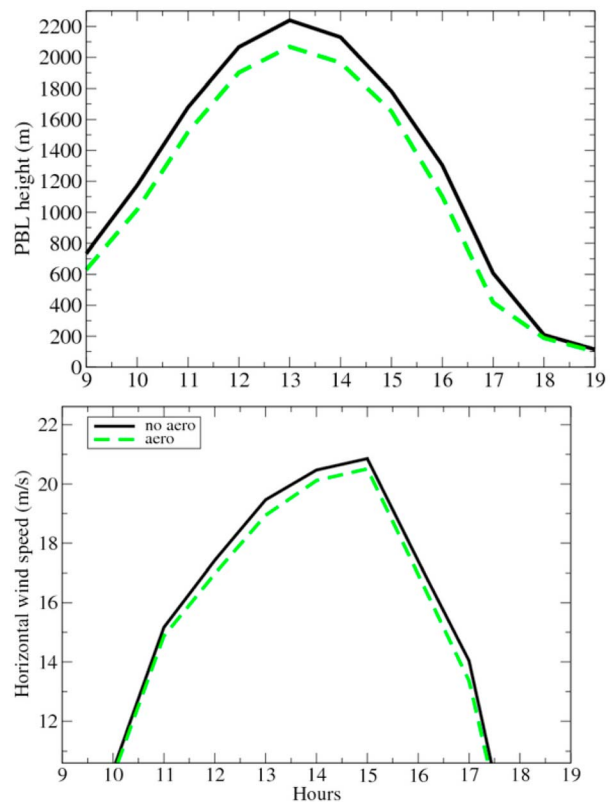


Figure 11. Diurnal cycles of (top) the planetary boundary layer (PBL) and (bottom) horizontal wind speed (integrated over the PBL height) simulated without and with aerosols.

result suggests a potential increase of the particulate concentration that could, in turn, strengthen its direct radiative forcing and its stabilizing effect in the planetary boundary layer (positive feedback).

4. Conclusions

[48] The main objectives of this work were (1) to estimate the ADRF of polluted aerosols during the heat wave of summer 2003 over western Europe and (2) to investigate the possible feedbacks of the ADRF on the regional climate by using an off-line coupling between the CHIMERE model (associated with an aerosol optical module) and the meteorological model WRF.

[49] Our simulations performed for the period 7–15 August 2003 clearly indicate that the presence of particles causes a significant reduction of solar radiation reaching the surface (mean $\Delta F_{\text{BOA}} = -(10\text{--}30) \text{ W/m}^2$) by reflection to space (mean $\Delta F_{\text{TOA}} = -(1\text{--}12) \text{ W/m}^2$) and by absorption of solar energy into the atmospheric layer (mean $\Delta F_{\text{atm}} = +(5\text{--}23) \text{ W/m}^2$). The maximum of ADRF is obtained over southeastern France, where the aerosol load is significant (mean $\text{AOT}_{\text{chimere}}(400 \text{ nm}) = 0.55\text{--}0.65$).

[50] Over southeastern France, the ADRF induces a decrease of near-surface air temperature (in average during the period studied) reaching $0.30 \pm 0.06 \text{ K}$. Moreover, the perturbation of the Earth's surface radiative balance due to the presence of particles leads to a reduction, during daytime, of both the sensible (16 W/m^2) and latent (21 W/m^2) heat fluxes emitted by the surface, which causes a radiative cooling of the air at the bottom of the PBL (up to 2.9 K/d at noon). In parallel, the absorption of solar radiation by aerosols induces a radiative warming within the PBL (up to 1.20 K/d at noon). Both effects cause a stabilization of the lower troposphere during daytime, which results in turn in a reduction of both the PBL height (8%–30%) and the horizontal wind speed (2%–6%) leading to a reduction of the air ventilation by 14%.

[51] This direct aerosol effect will have added a small contribution to the accumulation of particulate pollution observed in some European areas (Mediterranean Basin, P valley, etc.) during the heat wave of summer 2003 [Vautard et al., 2007a]. However, surface energy budget and atmospheric dynamics can also be sensitive to the aerosol indirect effect. In that sense, additional developments including aerosol impacts on cloud microphysics should be undertaken to investigate cloud feedback processes. In addition, future studies at higher spatial and temporal resolutions, associated with online aerosol module coupling, will help to highlight the possible feedback of the direct and indirect forcing on the PBL ventilation and associated air quality over urban-industrial areas. Furthermore, this work, focused on the regional climate feedbacks due to aerosol shortwave radiation interactions should be completed by the potential effect of dust and sea salt aerosols on longwave radiation.

[52] **Acknowledgments.** This work was funded by an INERIS/ANRT grant and the APIFLAME project (PRIMEQUAL). We would like to thank the AERONET and Baseline Surface Radiation Network (BSRN) teams for the use of their data. The authors also wish to thank the NOAA/NCEP-NCAR teams for providing the WRF model from their Web site at <http://www.mmm.ucar.edu/wrf/users/downloads.html>. Jean-Louis Monge is acknowledged for his support on issues related to WRF simulations.

References

- Bessagnet, B., A. Hodzic, R. Vautard, M. Beekmann, S. Cheinet, C. Honoré, C. Liousse, and L. Rouil (2004), Aerosol modeling with CHIMERE—Preliminary evaluation at the continental scale, *Atmos. Environ.*, **38**, 2803–2817.
- Bessagnet, B., L. Menut, G. Curci, A. Hodzic, B. Guillaume, C. Liousse, S. Moukhtar, B. Pun, C. Seigneur, and M. Schulz (2009), Regional modeling of carbonaceous aerosols over Europe—Focus on secondary organic aerosols, *J. Atmos. Chem.*, **61**, 175–202.
- Bond, T. C., G. Habib, and R. W. Bergström (2006), Limitations in the enhancement of visible light absorption due to mixing state, *J. Geophys. Res.*, **111**, D20211, doi:10.1029/2006JD007315.
- Boucher, O., et al. (1998), Intercomparison of models representing direct shortwave radiative forcing by sulfate aerosols, *J. Geophys. Res.*, **103**, 16,979–16,998.
- Calvo, A. I., V. Pont, A. Castro, M. Mallet, C. Palencia, J. C. Roger, P. Dubuisson, and R. Fraile (2010), Radiative forcing of haze during a forest fire in Spain, *J. Geophys. Res.*, **115**, D08206, doi:10.1029/2009JD012172.
- Chapman, E. G., W. I. Gustafson Jr., R. C. Easter, J. C. Barnard, S. J. Ghan, M. S. Pekour, and J. D. Fast (2009), Coupling aerosol-cloud-radiative processes in the WRF-Chem model: Investigating the radiative impact of elevated point sources, *Atmos. Chem. Phys.*, **9**, 945–964.
- Chen, F., and J. Dudhia (2001), Coupling an advanced land-surface/hydrology model with the Penn State/NCAR MM5 modeling system. Part 1: Model description and implementation, *Mon. Weather Rev.*, **129**, 569–585.
- Chou, M. D., and M. J. Suarez (1994), An efficient thermal infrared radiation parameterization for use in general circulation models, *NASA Tech. Memo., TM-104606*, vol. 3, 85 pp.
- d'Almeida, G. A., P. Koepke, and E. P. Shettle (1991), *Atmospheric Aerosols: Global Climatology and Radiative Characteristics*, A. Deepak, Hampton, Va.
- Dentener, F., et al. (2006), Emissions of primary aerosol and precursor gases in the years 2000 and 1750 prescribed data-sets for AeroCom, *Atmos. Chem. Phys.*, **6**, 4321–4344.
- Di Biagio, C. D., A. di Sarra, D. Meloni, F. Monteleone, S. Piacentino, and D. Sferlazzo (2009), Measurements of Mediterranean aerosol radiative forcing and influence of the single scattering albedo, *J. Geophys. Res.*, **114**, D06211, doi:10.1029/2008JD011037.
- Dubovik, O., and M. D. King (2000), A flexible inversion algorithm for retrieval of aerosol optical properties from Sun and sky radiance measurements, *J. Geophys. Res.*, **105**, 20,673–20,696.
- Dubovik, O., A. Smirnov, B. Holben, M. King, Y. Kaufman, T. Eck, and I. Slutsker (2000), Accuracy assessments of aerosol optical properties retrieved from Aerosol Robotic Network (AERONET) Sun and sky radiance measurements, *J. Geophys. Res.*, **105**, 9791–9806.
- Dubovik, O., B. Holben, T. F. Eck, A. Smirnov, Y. J. Kaufman, M. D. King, D. Tanré, and I. Slutsker (2002), Variability of absorption and optical properties of key aerosol types observed in worldwide locations, *J. Atmos. Sci.*, **59**, 590–608.
- Elias, T., and J. L. Roujean (2008), Estimation of the aerosol radiative forcing at ground level, over land, and in cloudless atmosphere, from METEOSAT-7 observation: Method and case study, *Atmos. Chem. Phys.*, **8**, 625–636.
- Fan, J., R. Zhang, W. K. Tao, and K. I. Mhor (2008), Effects of aerosol optical properties on deep convective clouds and radiative forcing, *J. Geophys. Res.*, **113**, D08209, doi:10.1029/2007JD009257.
- Fast, J. D., W. I. Gustafson Jr., R. C. Easter, R. A. Zaveri, J. C. Barnard, E. G. Chapman, G. A. Grell, and S. E. Peckham (2006), Evolution of ozone, particulates, and aerosol direct radiative forcing in the vicinity of Houston using a fully coupled meteorology-chemistry-aerosol model, *J. Geophys. Res.*, **111**, D21305, doi:10.1029/2005JD006721.
- Forster, P., et al. (2007), Changes in atmospheric constituents and in radiative forcing, in *Climate Change 2007: The Physical Science Basis. Contribution of Working Group I to the Fourth Assessment Report of the Intergovernmental Panel on Climate Change*, edited by S. Solomon et al., pp. 131–234, Cambridge Univ. Press, New York.
- Gong, D. Y., C. H. Ho, D. Chen, Y. Quian, Y. S. Choi, and J. Kim (2007), Weekly cycle of aerosol-meteorology interaction over China, *J. Geophys. Res.*, **112**, D22202, doi:10.1029/2007JD008888.
- Guenther, A., T. Karl, P. Harley, C. Wiedinmyer, P. I. Palmer, and C. Geron (2006), Estimates of global terrestrial isoprene emissions using MEGAN (Model of Emissions of Gases and Aerosols from Nature), *Atmos. Chem. Phys.*, **6**, 3181–3210.
- Guerova, G., and N. Jones (2007), A global model study of ozone enhancement during the August 2003 heat wave in Europe, *Environ. Chem.*, **4**, 285–292.

- Hess, M., P. Koepke, and I. Schult (1998), Optical properties of aerosols and clouds: The software package OPAC, *Bull. Am. Meteorol. Soc.*, **79**, 831–844.
- Hodzic, A., R. Vautard, B. Bessagnet, M. Lattuati, and F. Moreto (2005), Long-term urban aerosol simulation versus routine particulate matter observations, *Atmos. Environ.*, **39**, 5851–5864.
- Hodzic, A., R. Vautard, H. Chepfer, P. Goloub, L. Menut, P. Chazette, J. L. Deuzé, A. Apituley, and P. Couvert (2006), Evolution of aerosol optical thickness over Europe during the August 2003 heat wave as seen from CHIMERE model simulations and POLDER data, *Atmos. Chem. Phys.*, **6**, 1853–1864.
- Hodzic, A., S. Madronich, B. Bohn, S. Massie, L. Menut, and C. Wiedinmyer (2007), Wildfire particulate matter in Europe during summer 2003: Mesoscale modeling of smoke emissions, transport and radiative effects, *Atmos. Chem. Phys.*, **7**, 4043–4064.
- Hohenegger, C., and P. L. Vidale (2005), Sensitivity of the European climate to aerosol forcing as simulated with a regional climate model, *J. Geophys. Res.*, **110**, D06201, doi:10.1029/2004JD005335.
- Holben, B. N., et al. (2001), An emerging ground-based aerosol climatology: Aerosol optical depth from AERONET, *J. Geophys. Res.*, **106**, 12,067–12,097.
- Holzworth, G. C. (1972), Mixing heights, wind speeds, and potentials for urban air pollution throughout the contiguous United States, *Off. Air Publ. AP-101*, U.S. Environ. Prot. Agency, Research Triangle Park, N. C.
- Hong, S. Y. (2007), Stable boundary layer mixing in a vertical diffusion scheme, paper presented at The Korea Meteorological Society fall conference, Seoul, 25–26 Oct.
- Hong, S. Y., Y. Noh, and J. Dudhia (2006), A new vertical diffusion package with an explicit treatment of entrainment processes, *Mon. Weather Rev.*, **134**, 2318–2341.
- Honoré, C., et al. (2008), Predictability of European air quality: Assessment of 3 years of operational forecasts and analyses by the PREV^{AIR} system, *J. Geophys. Res.*, **113**, D04301, doi:10.1029/2007JD008761.
- Horowitz, L. W., S. Walters, D. Z. Mauzeralles, L. K. Emmonds, P. J. Rash, C. Granier, X. Tie, J. F. Lamarque, and M. G. Schultz (2003), A global simulation of tropospheric ozone and related tracers: Description and evaluation of MOZART, version 2, *J. Geophys. Res.*, **108**(D24), 4784, doi:10.1029/2002JD002853.
- Huebert, B. J., T. Bates, P. B. Russell, G. Shi, Y. J. Kim, K. Kawamura, G. Carmichael, and T. Nakajima (2003), An overview of ACE-Asia: Strategies for quantifying the relationships between Asian aerosols and their climatic impacts, *J. Geophys. Res.*, **108**(D23), 8633, doi:10.1029/2003JD003550.
- Junker, C., and C. Liousse (2008), A global emission inventory of carbonaceous aerosol from historic record of fossil fuel and biofuel consumption for the period 1860–1997, *Atmos. Chem. Phys.*, **8**, 1195–1207.
- Kain, J. S. (2004), The Kain–Fritsch convective parameterization: An update, *J. Appl. Meteorol.*, **43**, 170–181.
- Kalnay, E., et al. (1996), The NCEP/NCAR 40-year reanalysis project, *Bull. Am. Meteorol. Soc.*, **77**, 437–471.
- Kalnay, E., S. J. Lord, and R. D. McPherson (1998), Maturity of operational numerical weather prediction: Medium range, *Bull. Am. Meteorol. Soc.*, **79**, 2753–2892.
- Kedia, S., S. Ramachandran, A. Kumar, and M. M. Sarin (2010), Spatio-temporal gradients in aerosol radiative forcing and heating rate over Bay of Bengal and Arabian Sea derived on the basis of optical, physical, and chemical properties, *J. Geophys. Res.*, **115**, D07205, doi:10.1029/2009JD013136.
- Keil, A., and J. M. Haywood (2003), Solar radiative forcing by biomass burning aerosol particles during SAFARI 2000: A case study based on measured aerosol and cloud properties, *J. Geophys. Res.*, **108**(D13), 8467, doi:10.1029/2002JD002315.
- Konaré, A., A. S. Zakey, F. Solmon, F. Giorgi, S. Rauscher, S. Ibrah, and X. Bi (2008), A regional climate modeling study of the effect of desert dust on the West African monsoon, *J. Geophys. Res.*, **113**, D12206, doi:10.1029/2007JD009322.
- Krekov, G. M. (1993), *Aerosols Effects on Climate*, Univ. of Ariz. Press, Tucson.
- Kulmala, M., et al. (2011), General overview: European Integrated Project on Aerosol Cloud Climate and Air Quality Interactions (EUCAARI)—Integrating aerosol research from nano to global scales, *Atmos. Chem. Phys. Discuss.*, **11**, 17,941–18,160.
- Lack, D. A., C. D. Cappa, E. S. Cross, P. Massoli, A. T. Ahern, P. Davidovits, and T. B. Onasch (2009), Absorption enhancement of coated absorbing aerosols: Validation of the photo-acoustic technique for measuring the enhancement, *Aerosol Sci. Technol.*, **43**, 1006–1012.
- Lesins, G., P. Chylek, and U. Lohmann (2002), A study of internal and external mixing scenarios and its effect on aerosol optical properties and direct radiative forcing, *J. Geophys. Res.*, **107**(D10), 4094, doi:10.1029/2001JD000973.
- Li, Z., et al. (2007), Preface to special section on East Asian Studies of Tropospheric Aerosols: An International Regional Experiment (EAST-AIRE), *J. Geophys. Res.*, **112**, D22S00, doi:10.1029/2007JD008853.
- Loeb, N. G. (2010), Direct aerosol radiative forcing uncertainty based on a radiative perturbation analysis, *J. Clim.*, **23**, 5288–5293.
- Lyamani, H., F. J. Olmo, A. Alcantara, and L. Alados-Arboledas (2006), Atmospheric aerosols during the 2003 heat wave in southeastern Spain C: Microphysical columnar properties and radiative forcing, *Atmos. Environ.*, **40**, 6465–6476.
- Mallet, M., V. Pont, C. Liousse, J. C. Roger, and P. Dubuisson (2006), Simulation of aerosol radiative properties with the ORISAM-RAD model during a pollution event (ESCOMPTE 2001), *Atmos. Environ.*, **40**, 7696–7705.
- Mallet, M., P. Tulet, D. Serça, F. Solmon, O. Dubovik, J. Pelon, V. Pont, and O. Thouron (2009), Impact of dust aerosols on the radiative budget, surface heat fluxes, heating rate profiles and convective activity over West Africa during march 2006, *Atmos. Chem. Phys.*, **9**, 7143–7160.
- Marley, N. A., J. S. Gaffney, J. C. Baird, C. A. Blazer, P. J. Drayton, and J. E. Frederick (2001), An empirical method for the determination of the complex refractive index of size-fractionated atmospheric aerosols for radiative transfer calculations, *Aerosol Sci. Technol.*, **34**, 535–549.
- Märmer, E., B. Langmann, K. Hungershofer, and T. Trautmann (2007), Aerosol modeling over Europe: 2. Interannual variability of aerosol shortwave direct radiative forcing, *J. Geophys. Res.*, **112**, D23S16, doi:10.1029/2006JD008040.
- Mashayekhi, R., P. Irannejad, J. Feichter, and A. A. Bidokhti (2009), Implementation of a new aerosol HAM model within the Weather Research and Forecasting (WRF) modeling system, *Geosci. Model Dev. Discuss.*, **2**, 681–707.
- Matsui, T., A. Beltrán-Przekurat, D. Niyogi, R. A. Pielke Sr., and M. Coughenou (2008), Aerosol light scattering effect on terrestrial plant productivity and energy fluxes over the eastern United States, *J. Geophys. Res.*, **113**, D14S14, doi:10.1029/2007JD009658.
- Mercado, L. M., N. Bellouin, S. Sitch, O. Boucher, C. Huntingford, M. Wild, and P. M. Cox (2009), Impact of changes in diffuse radiation on the global land carbon sink, *Nature*, **458**, 1014–1017, doi:10.1038/nature07949.
- Meywerk, J., and V. Ramanathan (2002), Influence of anthropogenic aerosols on the total and spectral irradiance at the sea surface during the Indian Ocean Experiment (INDOEX) 1999, *J. Geophys. Res.*, **107**(D19), 8018, doi:10.1029/2000JD000022.
- Mlawer, E., S. Taubman, P. Brown, M. Iacono, and S. Clough (1997), Radiative transfer for inhomogeneous atmospheres: RRTM, a validated correlated-k model for the longwave, *J. Geophys. Res.*, **102**, 16,633–16,682.
- Molina, L. T., et al. (2010), An overview of the MILAGRO 2006 campaign: Mexico City emissions and their transport and transformation, *Atmos. Chem. Phys.*, **10**, 8697–8760.
- Monahan, E. C. (1986), The ocean as a source of atmospheric particles, in *The Role of Air–Sea Exchange in Geochemical Cycling*, pp. 129–163, Kluwer Acad., Dordrecht, Netherlands.
- Monteiro, A., A. I. Miranda, C. Borrego, R. Vautard, J. Ferreira, and A. Perez (2007), Long-term assessment of particulate matter using CHIMERE model, *Atmos. Environ.*, **41**, 7726–7738.
- Norris, J. R., and M. Wild (2007), Trends in aerosol radiative effects over Europe inferred from observed cloud cover, solar “dimming,” and solar “brightening,” *J. Geophys. Res.*, **112**, D08214, doi:10.1029/2006JD007794.
- Pandithurai, G., S. Dipu, K. K. Dani, S. Tiwari, D. S. Bisht, P. C. S. Devara, and R. T. Pinker (2008), Aerosol radiative forcing during dust events over New Delhi, India, *J. Geophys. Res.*, **113**, D13209, doi:10.1029/2008JD009804.
- Park, S. U., H. J. Ahn, and M. S. Park (2010), Direct shortwave radiative forcing of the Asian dust aerosol on dust emission, *Theor. Appl. Climatol.*, **101**, 179–190.
- Péré, J. C., M. Mallet, B. Bessagnet, and V. Pont (2009), Evidence of the aerosol core-shell mixing state over Europe during the heat wave of summer 2003 by using CHIMERE simulations and AERONET inversions, *Geophys. Res. Lett.*, **36**, L09807, doi:10.1029/2009GL037334.
- Péré, J. C., M. Mallet, V. Pont, and B. Bessagnet (2010), Evaluation of an aerosol optical scheme in the chemistry-transport model CHIMERE, *Atmos. Environ.*, **44**, 3688–3699.
- Pun, B., C. Seigneur, and K. Lohman (2006), Modeling secondary organic aerosol via multiphase partitioning with molecular data, *Environ. Sci. Technol.*, **40**, 4722–4731.
- Rajeev, K., K. Parameswaran, B. V. Thampi, M. K. Mishra, A. K. M. Nair, and S. Meenu (2010), Altitude distribution of aerosols over southeast Arabian Sea coast during pre-monsoon season: Elevated layers, long-

- range transport and atmospheric radiative heating, *Atmos. Environ.*, *44*, 2597–2604.
- Ramanathan, V. (2001), Indian Ocean Experiment: An integrated analysis of the climate forcing and effects of the great Indo-Asian haze, *J. Geophys. Res.*, *106*, 28,371–28,398.
- Ramanathan, V., and G. Carmichael (2008), Global and regional climate changes due to black carbon, *Nat. Geosci.*, *1*, 221–227.
- Randles, C. A., and V. Ramaswamy (2010), Direct and semi-direct impacts of absorbing biomass burning aerosol on the climate of southern Africa: A Geophysical Fluid Dynamics Laboratory GCM sensitivity study, *Atmos. Chem. Phys.*, *10*, 9819–9831.
- Redelsperger, J. L., C. Thorncroft, A. Diedhiou, T. Lebel, D. J. Parker, and J. Polcher (2006), African Monsoon Multidisciplinary Analysis (AMMA), an international research project and field campaign, *Bull. Am. Meteorol. Soc.*, *87*, 1739–1746.
- Roger, J. C., M. Mallet, P. Dubuisson, H. Cachier, E. Vermote, O. Dubovik, and S. Despiou (2006), A synergetic approach for estimating the local direct aerosol forcing: Application to an urban zone during the Expérience sur Site pour Contraindre les Modèles de Pollution et de Transport d'Emission (ESCOMPTE) experiment, *J. Geophys. Res.*, *111*, D13208, doi:10.1029/2005JD006361.
- Saha, A., M. Mallet, J. C. Roger, P. Dubuisson, J. Piazzola, and S. Despiou (2008), One year measurements of aerosol optical properties over an urban coastal site: Effect on local direct radiative forcing, *Atmos. Res.*, *90*, 195–202.
- Santos, D., M. J. Costa, and A. M. Silva (2008), Direct SW aerosol radiative forcing over Portugal, *Atmos. Chem. Phys.*, *8*, 5771–5786.
- Schmidt, H., C. Derognat, R. Vautard, and M. Beekmann (2001), A comparison of simulated and observed ozone mixing ratios for the summer of 1998 in western Europe, *Atmos. Environ.*, *35*, 6277–6297.
- Schmidt, K. S., et al. (2010), A new method for deriving aerosol solar radiative forcing and its first application within MILAGRO/INTEX-B, *Atmos. Chem. Phys.*, *10*, 7829–7843.
- Shindell, D., and G. Faluvegi (2009), Climate response to regional radiative forcing during the twentieth century, *Nat. Geosci.*, *2*, 294–300.
- Shiraiwa, M., Y. Kondo, T. Iwamoto, and K. Kita (2009), Amplification of light absorption of black carbon by organic coating, *Aerosol Sci. Technol.*, *44*, 46–54.
- Skamarock, W. C., J. B. Klemp, and J. Dudhia (2001), Prototypes for the WRF (Weather Research and Forecasting) model, paper presented at the Ninth Conference on Mesoscale Processes, Am. Meteorol. Soc., Fort Lauderdale, Fla.
- Solmon, F., M. Mallet, N. Elguindi, F. Giorgi, A. Zakey, and A. Konaré (2008), Dust aerosol impact on regional precipitation over western Africa, mechanisms and sensitivity to absorption properties, *Geophys. Res. Lett.*, *35*, L24705, doi:10.1029/2008GL035900.
- Takamura, T., N. Sugimoto, A. Shimizu, A. Uchiyama, A. Yamazaki, K. Aoki, T. Nakajima, B. J. Sohn, and H. Takenaka (2007), Aerosol radiative characteristics at Gosan, Korea, during the Atmospheric Brown Cloud East Asian Regional Experiment 2005, *J. Geophys. Res.*, *112*, D22S36, doi:10.1029/2007JD008506.
- Textor, C., et al. (2006), Analysis and quantification of the diversities of aerosol life cycles within AeroCom, *Atmos. Chem. Phys.*, *6*, 1777–1813.
- Trenberth, K. E., J. T. Fasullo, and J. Kiehl (2009), Earth's global energy budget, *Bull. Am. Meteorol. Soc.*, *90*, 311–323.
- Tummon, F., F. Solmon, C. Lioussé, and M. Tadross (2010), Simulation of the direct and semidirect aerosol effects on the southern Africa regional climate during the biomass burning season, *J. Geophys. Res.*, *115*, D19206, doi:10.1029/2009JD013738.
- Vautard, R., M. Beekmann, J. Roux, and D. Gombert (2001), Validation of a hybrid forecasting system for the ozone concentrations over the Paris area, *Atmos. Environ.*, *14*, 2449–2461.
- Vautard, R., et al. (2003), Paris emission inventory diagnostics from ESQUIF airborne measurements and a chemistry-transport model, *J. Geophys. Res.*, *108*(D17), 8564, doi:10.1029/2002JD002797.
- Vautard, R., B. Bessagnet, M. Chin, and L. Menut (2005a), On the contribution of natural aeolian sources to particulate matter concentrations in Europe: Testing hypotheses with a modeling approach, *Atmos. Environ.*, *39*, 3291–3303.
- Vautard, R., C. Honoré, M. Beekmann, and L. Rouil (2005b), Simulation of ozone during the August 2003 heat wave and emission control scenarios, *Atmos. Environ.*, *39*, 2957–2967.
- Vautard, R., M. Beekmann, J. Desplat, A. Hodzic, and S. Morel (2007a), Air quality in Europe during the summer of 2003 as a prototype of air quality in a warmer climate, *C. R. Geosci.*, *339*, 747–763.
- Vautard, R., et al. (2007b), Evaluation and intercomparison of ozone and PM10 simulations by several chemistry transport models over four European cities within the CityDelta project, *Atmos. Environ.*, *41*, 173–188.
- Wang, J., and S. A. Christopher (2006), Mesoscale modeling of Central American smoke transport to the United States: 2. Smoke radiative impact on regional surface energy budget and boundary layer evolution, *J. Geophys. Res.*, *111*, D14S92, doi:10.1029/2005JD006720.
- Wang, Y., H. Che, J. Ma, Q. Wang, G. Shi, H. Chen, P. Goloub, and X. Hao (2009), Aerosol radiative forcing under clear, hazy, foggy, and dusty weather conditions over Beijing, China, *Geophys. Res. Lett.*, *36*, L06804, doi:10.1029/2009GL037181.
- Wendisch, M., et al. (2008), Radiative and dynamic effects of absorbing aerosol particles over the Pearl River Delta, China, *Atmos. Environ.*, *42*, 6405–6416.
- Wu, Z. P., and Y. P. Wang (1991), Electromagnetic scattering for multilayered spheres: Recursive algorithms, *Radio Sci.*, *26*, 1393–1401.
- Yu, H., et al. (2006), A review of measurement-based assessments of the aerosol direct radiative effect and forcing, *Atmos. Chem. Phys.*, *6*, 613–666.
- Zanis, P. (2009), A study on the direct effect of anthropogenic aerosols on near surface air temperature over southeastern Europe during summer 2000 based on regional climate modeling, *Ann. Geophys.*, *27*, 3977–3988.
- Zhang, R., A. F. Khalizov, J. Pagels, D. Zhang, H. Xue, and P. H. McMurry (2008), Variability in morphology, hygroscopicity and optical properties of soot aerosols during atmospheric processing, *Proc. Natl. Acad. Sci. U. S. A.*, *105*, 10,291–10,296.
- Zhang, Y., X. Y. Wen, and C. J. Jang (2010), Simulating chemistry-aerosol-cloud-radiation-climate feedbacks over the continental U.S. using the online-coupled Weather Research Forecasting Model with chemistry (WRF/Chem), *Atmos. Environ.*, *44*, 3568–3582.
- Zhao, C., X. Liu, L. R. Leung, B. Johnson, S. A. McFarlane, W. I. Gustafson Jr., J. D. Fast, and R. Easter (2010), The spatial distribution of mineral dust and its shortwave radiative forcing over North Africa: Modeling sensitivities to dust emissions and aerosol size treatments, *Atmos. Chem. Phys.*, *10*, 8821–8838.

B. Bessagnet and J. C. Péré, Institut National de l'Environnement Industriel et des Risques, Parc technologique Alata, F-60550 Verneuil en Halatte, France. (bertrand.bessagnet@ineris.fr; jean-christophe.pere@ineris.fr)

M. Mallet and V. Pont, Laboratoire d'Aérodologie, Université de Toulouse, CNRS, 14 Avenue Edouard Belin, F-31400 Toulouse, France. (malm@aero.obs-mip.fr; ponv@aero.obs-mip.fr)